



Research Article

Effectively improved ionic conductivity of montmorillonite clay nanoplatelets incorporated nanocomposite solid polymer electrolytes for lithium ion-conducting devices

Priyanka Dhatarwal¹ · R. J. Sengwa¹ · Shobhna Choudhary^{1,2}

© Springer Nature Switzerland AG 2018

Abstract

Synergistic effects of lithium salt concentration and inorganic nanofiller incorporation on the ionic conductivity of polymer blend matrix based nanocomposite solid polymer electrolytes (NSPEs) have been examined. The montmorillonite (MMT) clay nanoplatelets incorporated NSPE films based on poly(ethylene oxide) and poly(methyl methacrylate) blend matrix with lithium tetrafluoroborate (LiBF_4) ionic salt have been prepared by the solution-cast method followed by melt-press technique. The 1, 3, and 5 wt% MMT amounts along with 13.3 wt% LiBF_4 amount as compared to the weight of polymer blend have been used for the preparation of NSPE films. X-ray diffractometer (XRD) and the Fourier transform infrared (FTIR) spectrometer have been employed for structural characterization of these NSPE films. The complex permittivity and ac electrical conductivity spectra are investigated by using the dielectric relaxation spectroscopy, whereas the electrochemical performance of these materials has been characterized by the electrochemical analyzer. The XRD patterns reveal that the NSPEs are predominantly amorphous and have the intercalated and exfoliated MMT platelets, whereas the relative changes in their FTIR spectra confirm the ion–dipolar–nanofiller interactions between the functional groups of the blended polymers, lithium ions, and the MMT nanoplatelets. The permittivity and conductivity spectra of these materials are analyzed for exploring the dominant contribution of electrode polarization and dipolar polarization in the low and high frequency regions, respectively, and the presence of relaxation processes associated with structural dynamics of the solid-state ion–dipolar complexes. It has been found that the NSPE of relatively fast polymer chain segmental dynamics exhibits higher ionic conductivity. The room temperature ionic conductivity of the 13.3 wt% LiBF_4 containing SPE is found more than two times higher as compared to that of the SPE film having 9.7 wt% LiBF_4 . When the MMT is incorporated, the ionic conductivity of 13.3 wt% LiBF_4 containing NSPEs enhances by about one order of magnitude at room temperature. The dc ionic conductivity of the 13.3 wt% LiBF_4 containing SPE film is found 1×10^{-5} S/cm at 55 °C, whereas it is 1.65×10^{-5} S/cm at 27 °C for the 5 wt% MMT incorporated NSPE film. The significantly enhanced ionic conductivity with ions transference number close to unity, high electrochemical stability voltage window and good reversibility of these NSPE materials confirm their potential applications as ion conductor/separator for the development of all-solid-state ion conducting devices and the lithium-ion batteries.

Keywords Solid polymer electrolyte · Inorganic nanofiller · Dielectric properties · Ionic conductivity · Structural dynamics

✉ R. J. Sengwa, rjsengwa@rediffmail.com; rjs.ph@jnvu.edu.in | ¹Dielectric Research Laboratory, Department of Physics, Jai Narain Vyas University, Jodhpur 342 005, India. ²CSIR-National Institute of Science Communication and Information Resources, New Delhi 110 012, India.

1 Introduction

Among the various types of energy storing devices, the solid-state lithium-ion batteries (LIBs) have gained great success due to their promising commercial applications [1–3]. The overall performance of the LIBs depends on the synergic properties of the electrodes (anode and cathode) and the electrolyte material used in their design and development [4–14]. The electrolyte material acts as an ion conductor/separator between the electrodes and governs most of the electrochemical parameters of a battery including its high-performance and safer workability. The solid polymer electrolytes (SPEs) [6–12, 14], inorganic solid electrolytes (ISEs) [13], hybrid solid polymer electrolytes (HSPEs) (i.e., inorganic materials incorporated nanocomposite solid polymer electrolytes (NSPEs) [15–19], and plasticized solid polymer electrolytes (PSPEs) [20–23]) are frequently used for the fabrication of high energy density rechargeable LIBs.

The relatively enhanced ionic conductivity, good flexibility, better electrode/electrolyte interface capability and excellent processability of the SPEs, NSPEs, and PSPEs are the main factors due to which these materials have been the topic of great interest for the researchers over the past few decades [6–12, 15–23]. So far, a large number of polymers and their blends as base matrices, different lithium metal salts as ionic dopant, various liquid plasticizers (high dielectric constant polar liquids for increasing amorphous phase and degree of salt dissolution), and a large number of nanosized inorganic materials (for improving the physical and electrochemical performance and to prevent the growth of dendrites during cycling) have been used for the preparation of novel SPE, NSPE and PSPE materials. In addition to their applications in LIBs [7, 10, 15, 22], these solid ion conducting materials have also been technologically recognized for the development of supercapacitors [23], dye-sensitized solar cells [24], fuel cells [25], and electrochromic devices including smart windows [26]. Basically, the SPEs, NSPEs, and PSPEs are flexible-type solid-state or quasi-solid-state ion–dipolar complexes in which ions transportation occurs coupled with dynamics of polymer chain segments mainly through the amorphous phases of the material [10, 17, 20, 27, 28]. Therefore, it is the prime goal of the researchers to prepare these complexes of amorphous nature with faster structural dynamics along with promising thermophysical properties for safe working of the battery when it is made of such novel ion conducting materials.

In the last few years, a variety of SPE, NSPE and PSPE films based on poly(ethylene oxide) (PEO), poly(methyl methacrylate) (PMMA) and their blend matrices have

been prepared through different preparation methods in our laboratory and these were characterized by employing various advanced techniques [29–40]. Lithium salts namely LiClO_4 , LiCF_3SO_3 and LiBF_4 ; plasticizers EC, PC and PEG; and inorganic nanofillers MMT, SiO_2 , Al_2O_3 , ZnO, and SnO_2 have been used for the preparation of SPE, NSPE, and PSPE materials. Significant variations have been noted in the structures, dielectric properties, structural relaxation processes, and ionic conductivity with the change of polymer matrix, ionic salt, plasticizer, and nanofiller of the investigated electrolyte materials so far [29–40]. In continuation of our ongoing work on the solid polymer electrolyte materials, this paper aims; firstly, to explore the variations in the dielectric and electrical properties of PEO–PMMA blend matrix based SPEs with LiBF_4 salt concentrations 9.7 wt% and 13.3 wt% at various temperatures, and secondly, to confirm the effect of incorporated MMT nanoplatelets on the structural dynamics and ionic conductivity of 13.3 wt% LiBF_4 containing NSPE films at room temperature, in order to confirm their potential applications in the energy storing devices and also for the lithium-ion conducting electrochromic devices.

2 Experimental

2.1 Materials and sample preparation

The PEO ($M_w = 6 \times 10^5 \text{ g mol}^{-1}$), PMMA ($M_w = 3.5 \times 10^5 \text{ g mol}^{-1}$), LiBF_4 and MMT nanoclay (PGV; Nanocor[®]) were obtained from Sigma-Aldrich, USA. Acetonitrile and tetrahydrofuran of spectroscopic grade were purchased from Loba Chemie, India and used as solvents. The MMT nanoclay is white in colour, and has 145 mequiv./100 g cation exchange capacity (CEC), 2.6 g/cc specific gravity, 9–10 pH value (5% dispersion), and the layered sheets (platelets) of one-nanometer thickness with 150–200 aspect ratio (length/width), which are stacked by weak dipolar and van der Waals forces, and it exhibits intercalated and exfoliated phases when dispersed in the polar polymer matrix as given in the technical data sheet of the manufacturer. For the preparation of SPE and NSPE films by the solution-cast method, equal weight amounts of PEO and PMMA each of 1 g, 0.2658 g LiBF_4 for 13.3 wt% concentration of the salt, and 0.02, 0.06 and 0.10 g amounts of MMT for its 1, 3 and 5 wt% concentrations with respect to 2 g amount of the polymer blend (PEO–PMMA) were used. The 13.3 wt% concentration of LiBF_4 in these electrolyte films is equal to the stoichiometric molar ratio 12:1 of total dipolar groups ($\text{E}\ddot{\text{O}} + (\text{C}=\ddot{\text{O}})$) to the salt cations (Li^+), where $\text{E}\ddot{\text{O}}$ is the ether oxygen of ethylene oxide repeat unit of the PEO and $\text{C}=\ddot{\text{O}}$ is the carbonyl group of PMMA monomer unit.

Initially, the required amounts of PEO and PMMA were dissolved in acetonitrile and tetrahydrofuran separately in glass bottles, and then these were mixed together. After that, the amounts of LiBF_4 was added and it was dissolved under magnetic stirring, and then the amount of MMT for x wt% was added and the same was homogeneously dispersed under vigorous magnetic stirring. The solutions for all the samples of varying MMT concentrations (x wt%) were prepared by following the same steps as reported above. These electrolyte solutions were cast on to Teflon petri dishes and after solvent evaporation, the free-standing flexible-type NSPE films were obtained. These solution-cast NSPE films were vacuum dried and then the surfaces of these electrolyte films were made smooth by the hot-press technique using the polymer press film making unit (Technosearch Instruments; Model PF-M15). The SPE film (PEO–PMMA)–9.7 wt% LiBF_4 of stoichiometric molar ratio i.e., $(\text{E}\ddot{\text{O}} + \text{C}=\ddot{\text{O}}): \text{Li}^+ = 16:1$ was prepared and studied in our previous paper [40] and its temperature dependent results have been used for its comparison with 12:1 stoichiometric molar ratio (PEO–PMMA)–13.3 wt% LiBF_4 film. Here it may be noted that for the higher salt concentration of SPE film, its stoichiometric molar ratio is low.

2.2 Characterizations

2.2.1 Structural measurements

The XRD patterns of the NSPE films were recorded in reflection mode of Cu K α radiation ($\lambda = 1.5406 \text{ \AA}$) over the angular range $3.8^\circ \leq 2\theta \leq 30^\circ$ with a scan rate of $0.05^\circ/\text{s}$. PANalytical X'pert Pro MPD X-ray diffractometer (XRD) operated at 1800 W (45 kV and 40 mA) was used for recording the XRD patterns at room temperature. The FTIR spectra of these films were recorded in ATR mode over the wavenumber range $650\text{--}4000 \text{ cm}^{-1}$ using Agilent technologies FTIR spectrometer (Cary 630), at room temperature.

2.2.2 Dielectric and electrical measurements

The complex permittivity and electrical conductivity spectra of the electrolyte films were determined by measurements of the parallel circuit capacitance C_p and resistance R_p under 1 V alternating current (ac) electric field. Agilent technologies 4284A precision LCR meter equipped with Agilent 16451B solid dielectric test fixture was used for the measurements of C_p and R_p in the frequency range of 20 Hz–1 MHz at 27°C for the NSPEs and also for the SPE film without nanofiller with temperature variation over the range $27\text{--}55^\circ\text{C}$. All measurements were made by placing the test fixture in a microprocessor controlled oven with $\pm 0.5^\circ\text{C}$ stability of temperature.

2.2.3 Electrochemical measurements

The linear sweep voltammetry (LSV), cyclic voltammetry (CV) and chronoamperometry (CA) of these NSPE films at room temperature were carried out by employing the electrochemical analyzer (CH Instruments, Inc. CHI 608E). The measurements were made with stainless steel (SS) blocking electrodes symmetrical cell (S-cell) assembly i.e., the SS||electrolyte||SS cell at room temperature.

3 Results and discussion

3.1 Structural behaviour

3.1.1 XRD patterns

The XRD patterns of LiBF_4 powder and (PEO–PMMA)–13.3 wt% LiBF_4 – x wt% MMT films along with the (PEO–PMMA)–9.7 wt% LiBF_4 film studied earlier [40] are shown in Fig. 1. From the figure, it can be noted that the crystalline LiBF_4 exhibits intense characteristic diffraction peak at $2\theta = 26.33^\circ$ and several low-intensity peaks in the 2θ range $18^\circ\text{--}30^\circ$. The SPE films having LiBF_4 concentrations 9.7 wt% and 13.3 wt% exhibit the less intense diffraction peaks around 19° and 23° (exact values are given in Table 1) which attribute to PEO crystallites in these SPEs because the pristine PEO has characteristic diffraction peaks at 19.22° and 23.41° corresponding to its reflection planes (120) and concerted (112),(032), respectively [21, 41]. Further, it is also because the PMMA used is an amorphous material and it has no sharp crystalline diffraction peak and exhibits a broader halo [30], whereas the LiBF_4 peaks are absent due to its dissociation in the SPE and NSPE films. From these XRD patterns, it can be concluded that; firstly, the added amounts of LiBF_4 for both the concentrations (i.e., 9.7 wt% and 13.3 wt%) have completely dissolved; secondly, the crystalline phase of 9.7 wt% LiBF_4 containing SPE film is relatively high as evident from its greater intensity diffraction peaks; and thirdly, the overall crystalline phase of these films is very low as inferred from the very low intensities of their diffraction peaks as compared to that of the pristine PEO peaks intensities (values of intensities I are given in Table 1 [41]) which confirm that these SPEs of different LiBF_4 concentrations are predominantly amorphous.

The exact values of the degree of crystallinity X_c (%) of these electrolyte materials were determined using the relation $X_c (\%) = (A_p / (A_p + A_H)) \times 100$, where A_p and A_H are the crystalline peaks and hump areas as highlighted in Fig. 1b for 5 wt% MMT containing NSPE film as a representative depiction. The A_p and A_H values for these films were determined using OriginPro® version-8 software. The

Fig. 1 **a** XRD patterns of LiBF₄ salt, (PEO–PMMA)–13.3 wt% LiBF₄–*x* wt% MMT films of stoichiometric molar ratio 12:1 and (PEO–PMMA)–9.7 wt% LiBF₄ film of stoichiometric molar ratio 16:1; **b** the enlarged view of the XRD pattern of (PEO–PMMA)–13.3 wt% LiBF₄–5 wt% MMT film with the highlighted areas of peaks (solid cyan color) and hump (pumpkin color with slanted lines); and **c** plot of *X_c* versus *x* wt% MMT of the NSPE films

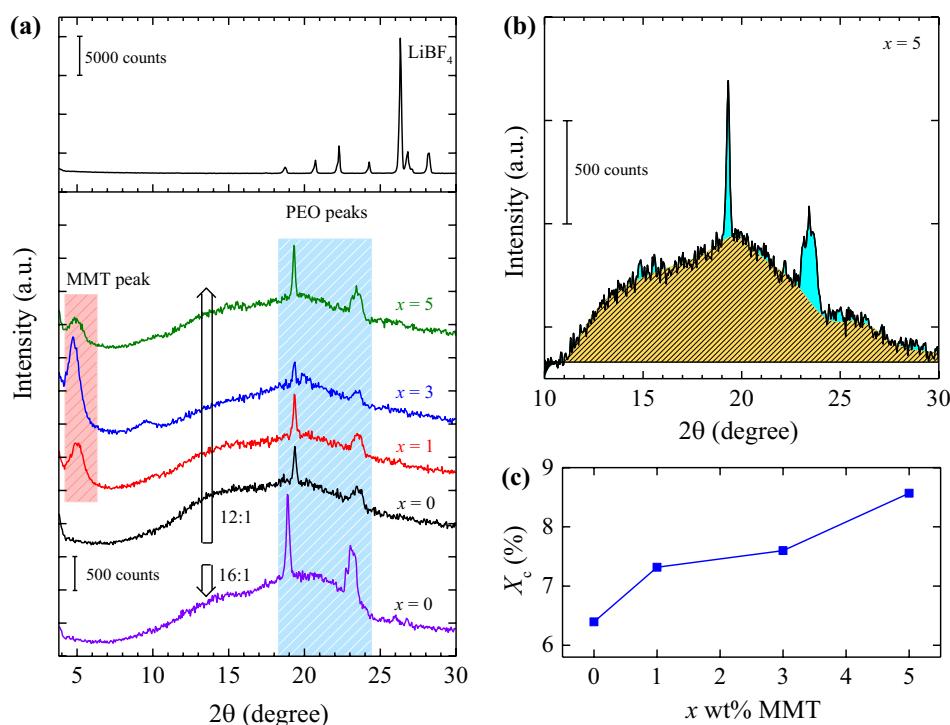


Table 1 Values of Bragg’s angle 2θ , basal spacing d , full width at half maximum FWHM, crystallite size L , crystalline peak intensity I and relative intensity R/I of MMT powder [41], pristine PEO film [41] and (PEO–PMMA)–13.3 wt% LiBF₄–*x* wt% MMT films

<i>x</i> wt% MMT	2θ (°)	d (nm)	FWHM $\times 10^3$ (rad)	L (nm)	I (counts)	R/I (%)
MMT (001) reflection peak parameters in the NSPE films						
MMT	7.03	1.257	17.19	8.44	520	100
1	5.03	1.757	14.08	10.29	460	88
3	4.79	1.843	12.81	11.31	909	175
5	4.82	1.833	14.75	9.83	265	51
PEO (120) reflection peak parameters in the NSPE films						
PEO	19.22	0.4614	4.70	31.28	12,964	100
0	19.37	0.4579	3.93	37.41	542	4.18
1	19.35	0.4585	3.74	39.33	648	5.00
3	19.33	0.4589	3.96	37.08	356	2.75
5	19.31	0.4592	3.44	42.72	769	5.93
PEO (112), (032) reflection peak parameters in the NSPE films						
PEO	23.41	0.3796	13.13	11.27	12,569	100
0	23.47	0.3788	14.33	10.32	329	2.62
1	23.49	0.3785	13.30	11.12	286	2.28
3	23.62	0.3764	10.42	14.20	195	1.55
5	23.43	0.3794	13.33	11.09	419	3.33

X_c values of 13.3 wt% and 9.7 wt% LiBF₄ containing SPE films were found 6.4% and 10.9%, respectively. The variation of *X_c* with MMT concentrations of the NSPE films are depicted in Fig. 1c. From this plot, it can be noted that the crystallinity of the NSPE films is very small and it unsystematically increases with the increase of MMT concentration.

Figure 1a shows that the XRD patterns of NSPE films containing 13.3 wt% LiBF₄ and 1, 3 or 5 wt% MMT exhibit

the intercalated MMT peak around 5° (exact 2θ values for these NSPEs are given in Table 1). The pristine MMT exhibits (001) reflection plane peak at 7.03° [41] and this peak is observed at a lower angle (~5°) for NSPEs which confirms the presence of intercalated MMT phase in these NSPE materials. But the significant variation in (001) peak intensity with the increase of incorporated MMT amounts in the NSPEs also infers that beside the

intercalated structures, there is also the presence of exfoliated MMT structures.

In order to get further insights into the structures of these NSPE films, the values of basal spacing d and crystallite size L of the MMT and the PEO crystallites in the NSPEs were determined by using the Bragg's relation $\lambda = 2d \sin\theta$ and the Scherrer's equation $L = 0.94\lambda/\beta\cos\theta$, respectively, and the observed d and L values as a function of x wt% MMT are recorded in Table 1. Figure 2 shows the variation of L , d , and RI (RI is the relative intensity of the intercalated MMT peak of NSPE films in comparison to the peak intensity of pristine MMT powder) as a function of x wt% MMT of the NSPE films. From this figure, it can be noted that the d values of MMT in the NSPEs enhance by about 0.5 nm which confirms that at least one layer of ion-dipolar complexes has entered into the MMT inter-layer galleries. Further, the L values show that the sizes of MMT crystallites have also increased in the NSPE materials which are maximum for 3 wt% MMT containing NSPE film. Figure 2 also infers that the (001) peak relative intensity (RI) greatly varies with the increase of MMT concentration and it is relatively high for 3 wt% MMT containing NSPE film confirming higher amount of MMT intercalated phase,

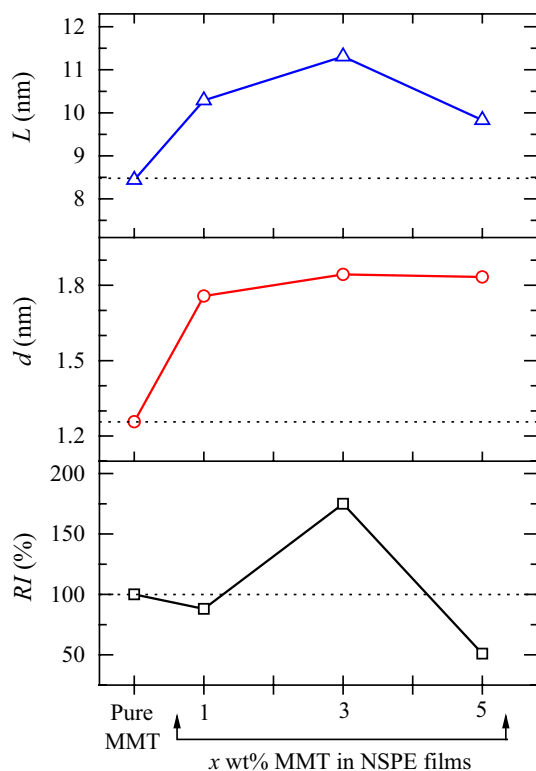


Fig. 2 The basal spacing d , crystallite size L , and relative intensity RI of the MMT nanofiller in the (PEO-PMMA)-13.3 wt% LiBF_4 - x wt% MMT nanocomposite electrolyte films. The d , L and RI values of pure MMT are taken from ref [41]

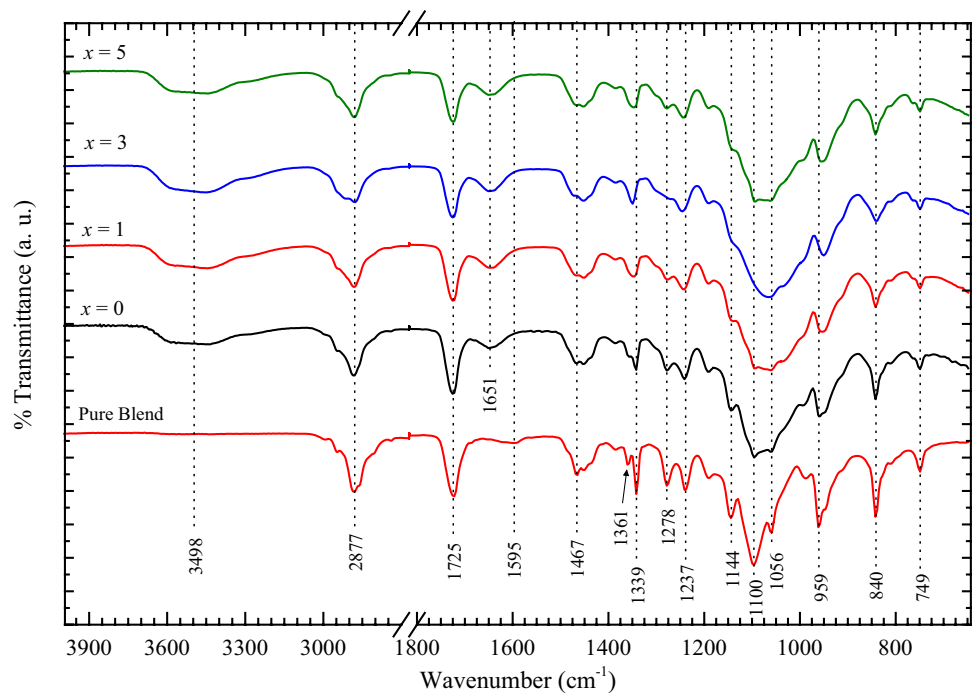
whereas the amount of this intercalated phase is relatively low for 5 wt% MMT containing NSPE film.

Table 1 shows that the values of d spacing corresponding to the (120) and (112),(032) reflection plane of PEO in the NSPE films are slightly lower than that of the pristine PEO, but the L values enhance although the amount of these crystallites in the NSPEs is very small as compared to that in the pristine PEO film. The significant changes in the structural parameters of MMT and PEO in these NSPE materials reveal that the structures of ion-dipolar complexes vary with the change of salt concentrations and also with the amount of incorporated MMT which reflects that there is an alteration of the ion-dipolar, ion-nanofiller, polymer-nanofiller, and the ion-dipolar-nanofiller interactions.

3.1.2 FTIR spectra

The FTIR spectra of (PEO-PMMA)-13.3 wt% LiBF_4 - x wt% MMT films over the wavenumber range 650–4000 cm^{-1} are depicted in Fig. 3. In order to examine the ion-dipolar and ion-dipolar-MMT interactions in the electrolytes, the FTIR spectrum of pure PEO-PMMA blend (50/50 wt%) which has been used as a base matrix for the preparation of SPE and NSPE films, is also given in Fig. 3 with the marking of wavenumbers corresponding to its various vibrational bands. The FTIR spectra of all these materials do not have any prominent absorbance band in the intermediate wavenumber range, and therefore, the 1800–2700 cm^{-1} range part of the spectra has been omitted for stretching the scale of lower wavenumber in view of clear legibility of various characteristic bands. Several relative changes in the characteristic absorption bands of pristine polymers i.e., shape, intensity, and shift in position, and also the disappearance of certain bands and appearance of some new bands with the addition of ionic salt in the polymer blend and also the dispersion of nanofiller in these electrolyte films can be noticed from the relative inspection of these FTIR spectra. Firstly, it is noted that the FTIR spectrum of pure blend film exhibits the various characteristic bands of the pristine PEO and PMMA structures. Review of literature ascertains that the PEO chain structures exhibit the absorption bands corresponding to various vibrational modes of CH_2 group in the wavenumber range from 1470 to 1330 cm^{-1} and the C–O–C group in the vicinity of 1160–1050 cm^{-1} [14], whereas pristine PMMA chain structures display the characteristic absorbance peaks at about 1730 cm^{-1} , 1440 cm^{-1} and 1150 cm^{-1} for the stretching vibrations of C=O group, bending vibration of C–H bond in the CH_3 group in-plane, and the stretching vibration of C–O bond [19]. The alterations in these vibrational modes of the PEO and PMMA in their 50/50 wt% blend as can be seen from the wavenumber values marked in Fig. 3 are

Fig. 3 FTIR spectra of pure PEO–PMMA blend and (PEO–PMMA)–13.3 wt% LiBF₄–*x* wt% MMT films for *x* values 0, 1, 3, and 5. The wavenumbers of various vibrational bands are marked in the figure for pure PEO–PMMA blend film



due to heterogeneous polymer chain interactions which resulted the formation of the homogeneous and miscible blend as analyzed in detail in the earlier studies [18, 37, 40]. The shoulders peaks at 1144 cm⁻¹ and 1056 cm⁻¹ in the triplet of C–O–C stretching mode and the doublets at 1361 cm⁻¹ and 1339 cm⁻¹ of CH₂ wagging mode in the FTIR spectrum of PEO–PMMA blend ascertain the crystalline phase of PEO structures [14, 18].

The FTIR spectrum of SPE film (i.e., *x*=0 in Fig. 3) clearly shows that on the doping of 13.3 wt% LiBF₄ salt in the 50/50 wt% PEO–PMMA blend matrix results in a huge suppression of PEO crystallite bands and also a large broadening of central peak in triplet confirms the formation of strong ion–dipolar complexes which turns the electrolyte material predominantly into amorphous nature, and this finding is in good agreement of the XRD results. Further, the less intense peak of the PEO–PMMA band at 1595 cm⁻¹ is completely suppressed and a new band appeared at 1651 cm⁻¹ in the SPE film. These changes in the PEO and PMMA characteristic bands indicate that the cation of salt strongly interacts with the ether oxygens of the PEO chain and moderately with the carbonyl groups of PMMA chain. Further, the broad band centered at 3498 cm⁻¹ is exhibited in the FTIR of SPE film, which was not present in the spectrum of the pure blend, also confirming the presence of ions in the SPE film. The FTIR spectra of NSPE films (Fig. 3; *x*=1, 3, and 5) indicates that the dispersion of MMT reduces the intensity of C–H deformation band (840 cm⁻¹), shifted the C–O deformation band (959 cm⁻¹) with some changes in its intensity, some alteration in broadening

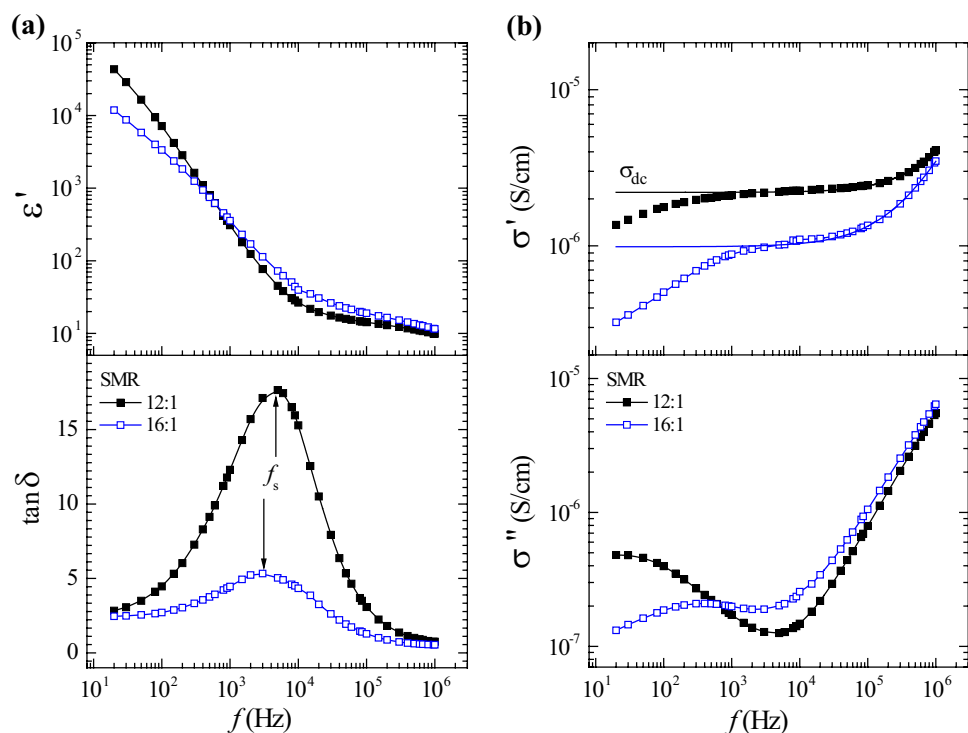
of C–O stretching band (1100 cm⁻¹), shift in C–H bending modes, and a relative decrease of C=O bending vibrational band intensity altogether confirms the interaction of dispersed MMT nanoplatelets with the ion–dipolar complexes of these nanocomposite electrolyte materials. The MMT exhibits a broad band corresponding to its Si–O stretching centered around 1040 cm⁻¹ which also coalesces with a broader band of C–O–C amorphous phase and produces some alteration in the shape and position of this band further indicating the interaction of the polymer with MMT platelet structures.

3.2 Dielectric and electrical conductivity spectra

3.2.1 Effect of salt concentration

The complex permittivity (real part ϵ') and dielectric loss tangent ($\tan\delta = \epsilon''/\epsilon'$) spectra of (PEO–PMMA)–13.3 wt% LiBF₄ film are shown in Fig. 4a, whereas Fig. 4b shows the complex ac electrical conductivity spectra (real part σ' and loss part σ''), at room temperature (27 °C). In order to explore the effect of salt concentration on the dielectric and electrical properties, the ϵ' , $\tan\delta$, σ' and σ'' spectra of (PEO–PMMA)–9.7 wt% LiBF₄ film investigated earlier in our laboratory [40] have also been included in Fig. 4. It can be noted from the figure that the ϵ' values sharply increase with the decrease of frequency in the low frequency region and finally attain the values higher than four orders of magnitude at 20 Hz. These high ϵ' values at low frequencies are due to dominant contribution of

Fig. 4 **a** The complex permittivity (real part ϵ') and dielectric loss tangent $\tan\delta$ (ϵ''/ϵ'), and **b** ac electrical conductivity (real part σ' and loss part σ'') spectra of (PEO–PMMA)–13.3 wt% LiBF₄ film of stoichiometric molar ratio 12:1 and (PEO–PMMA)–9.7 wt% LiBF₄ film of stoichiometric molar ratio 16:1. Stoichiometric molar ratio (SMR) represents the (E \ddot{O} +C=O): Li⁺ values of the SPEs



the electrode polarization (EP) effect which is a common behaviour of all the studied SPE materials [17, 19, 27, 29–35, 42–47]. Further, there is a gradual decrease in ϵ' values with the increase of frequency above 10 kHz and they finally approach a steady state around 1 MHz. The high frequency dispersion is attributed to the dipolar and ionic polarization in these solid ion–dipolar complexes.

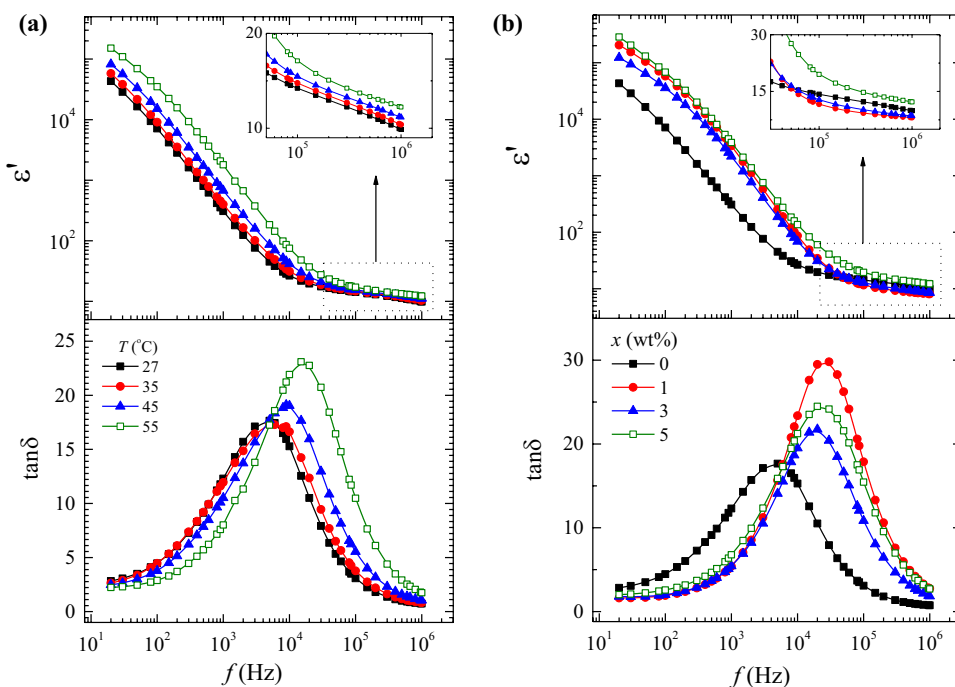
Figure 4a shows that at the start frequency of the ϵ' spectra (20 Hz), the ϵ' is about half order of magnitude high for the higher salt concentration (13.3 wt% LiBF₄) SPE film but it becomes slightly lower as compared to the low salt concentration (9.7 wt% LiBF₄) SPE film when the frequency exceeds 1 kHz. This result infers that the frequency dependent dielectric polarization of these SPE films are influenced by the salt concentration, and the contribution of polarization processes occurring at low, intermediate, and high frequency regions of the spectra also vary non-uniformly with the increase of salt concentration. Further, the $\tan\delta$ values (Fig. 4a) and σ' values (Fig. 4b) of 13.3 wt% LiBF₄ containing SPE film are very high as compared to that of the 9.7 wt% LiBF₄ containing SPE film. Figure 4a shows that there is a huge increase of $\tan\delta$ relaxation peak intensity with a small shift towards the high frequency side confirming that there is a large increase of dielectric losses in the ion–dipolar complexes and the dielectric relaxation process becomes fast for the relatively higher salt concentration SPE film. The results demonstrate that the increased ions concentration and enhanced structural dynamics of ion–dipolar complexes increases the ionic

conductivity of the SPE materials based on the same polymer matrix. The dc ionic conductivity ($\sigma_{dc} = 2.2 \times 10^{-6}$ S/cm) of the 13.3 wt% LiBF₄ containing SPE film is found 2.2 times higher than that of the 9.7 wt% LiBF₄ containing SPE film ($\sigma_{dc} = 1 \times 10^{-6}$ S/cm) at room temperature which were obtained from the power law fit of their σ' spectra as shown by solid lines in Fig. 4b. The σ'' spectra of these different salt concentrations SPE materials exhibit identical shapes but differ in their values on the frequency scale. The significance of these shapes of σ'' spectra in relation to the relaxation processes of the SPE material are considered in the next section.

3.2.2 Effect of temperature and MMT concentration

Figure 5a presents the ϵ' and $\tan\delta$ spectra of (PEO–PMMA)–13.3 wt% LiBF₄ SPE-film at different temperatures in the range 27–55 °C. It can be noticed that the ϵ' values increase with the increase of temperature of the SPE film. The increase of ϵ' values is found relatively high in the EP effect dominated low frequency region, whereas, in the dipolar and ionic polarization dominated high frequency region, the increase is relatively low which can be noted from the enlarged view of the high frequency region spectra as shown in the inset of the figure. Further, the $\tan\delta$ peak intensity also enhances and it gradually shifts towards the higher frequency side as the temperature of film increases. This type of ϵ' and $\tan\delta$ dispersion behaviour is expected because the increase of temperature creates

Fig. 5 The complex permittivity (real part ϵ') and dielectric loss tangent $\tan\delta$ (ϵ''/ϵ') spectra of **a** (PEO–PMMA)–13.3 wt% LiBF₄ SPE-film at various temperatures, and **b** (PEO–PMMA)–13.3 wt% LiBF₄–*x* wt% MMT NSPE-films at 27 °C



more free volume in the structures of solid ion–dipolar complexes which helps the dipoles to attain more ordered arrangement with the enhanced chain segmental dynamics which is in good agreement of the earlier results on different SPE materials [19, 31, 37, 44, 45, 47].

The effect of MMT concentration on the ϵ' and $\tan\delta$ values of the NSPE-films at a fixed temperature (27 °C) can be seen from Fig. 5b. It is observed that on the addition of 1 wt% MMT the ϵ' values of the NSPE-film significantly enhances as compared to the SPE film without MMT, but further variation in ϵ' values is relatively small and also change anomalously with the increase of MMT concentration up to 5 wt%. Inset of Fig. 5b shows the enlarged view of the ϵ' spectra of NSPEs in the high frequency region for a better understanding of the changes in high frequency dielectric polarization with MMT concentration.

The ϵ' values of the NSPE films at 10 kHz and 1 MHz frequencies are listed in Table 2 for their comparative analysis. The $\tan\delta$ peaks intensities of these NSPE films also enhance and exhibit a shift towards high frequency side as compared to the SPE film without MMT. The ϵ' values of all these NSPE materials have an abrupt change around 10 kHz and these values increase sharply with the decrease of frequency below this and gradually decrease with the increase of frequency above 10 kHz and finally approach the steady state near 1 MHz. Therefore, using the ϵ' values corresponding to 10 kHz and 1 MHz frequencies, the dielectric strength $\Delta\epsilon$ of the SPE film as a function of temperature and of the NSPE films as a function of MMT were estimated by the relation, $\Delta\epsilon = \epsilon'(10 \text{ kHz}) - \epsilon'(1 \text{ MHz})$ and the observed $\Delta\epsilon$ values for these materials are recorded in Table 2. It is found that the $\Delta\epsilon$ values of NSPEs are many

Table 2 Values of dielectric permittivity (real part) ϵ' ($\approx \epsilon_s$) at 10 kHz and ϵ' ($\approx \epsilon_\infty$) at 1 MHz, dielectric strength $\Delta\epsilon = \epsilon_s - \epsilon_\infty$, EDL relaxation time τ_{EDL} , polymer chain segmental dynamics relaxation time τ_s , dc ionic conductivity σ_{dc} and exponent factor *n* of the (PEO–PMMA)–13.3 wt% LiBF₄–*x* wt% MMT films at 27 °C, and the (PEO–PMMA)–13.3 wt% LiBF₄ film at various temperatures

	ϵ_s (10 kHz)	ϵ_∞ (1 MHz)	$\Delta\epsilon$	τ_{EDL} (ms)	τ_s (μ s)	σ_{dc} (μ S/cm)	<i>n</i>
<i>x</i> (wt %)	(PEO–PMMA)– 13.3 wt% LiBF ₄ – <i>x</i> wt% MMT films						
0	26.52	9.88	16.64	7.58	31.80	2.20	0.92
1	86.40	8.09	78.31	1.27	6.12	11.40	0.89
3	68.65	8.51	60.15	1.08	8.64	7.45	0.98
5	136.63	12.24	124.39	1.64	7.14	16.50	0.85
<i>T</i> (°C)	(PEO–PMMA)– 13.3 wt% LiBF ₄ film						
27	26.52	9.88	16.64	7.58	31.80	2.20	0.92
35	31.27	10.39	20.88	6.92	28.90	2.82	0.85
45	41.50	11.16	30.34	4.98	17.40	4.40	0.86
55	75.34	12.23	63.11	2.15	10.00	9.40	0.87

times greater than that of the SPE film at 27 °C, but these values show a gradual increase as the temperature of the SPE film increases (Table 2).

The values of relaxation time τ_s corresponding to the dynamics of ions coupled polymer chain segments in the solid ion–dipolar complexes of these electrolyte materials have been determined from the values of $\tan\delta$ peak frequency f_s using the relation $\tau_s = 1/2\pi f_s$, and the observed τ_s values of the SPE film with temperature variation and the NSPE films with x wt% MMT, at 27 °C, are recorded in Table 2. The dependence of dc ionic conductivity values of the SPE and NSPE films on their $\Delta\epsilon$ and τ_s values is discussed in the later section.

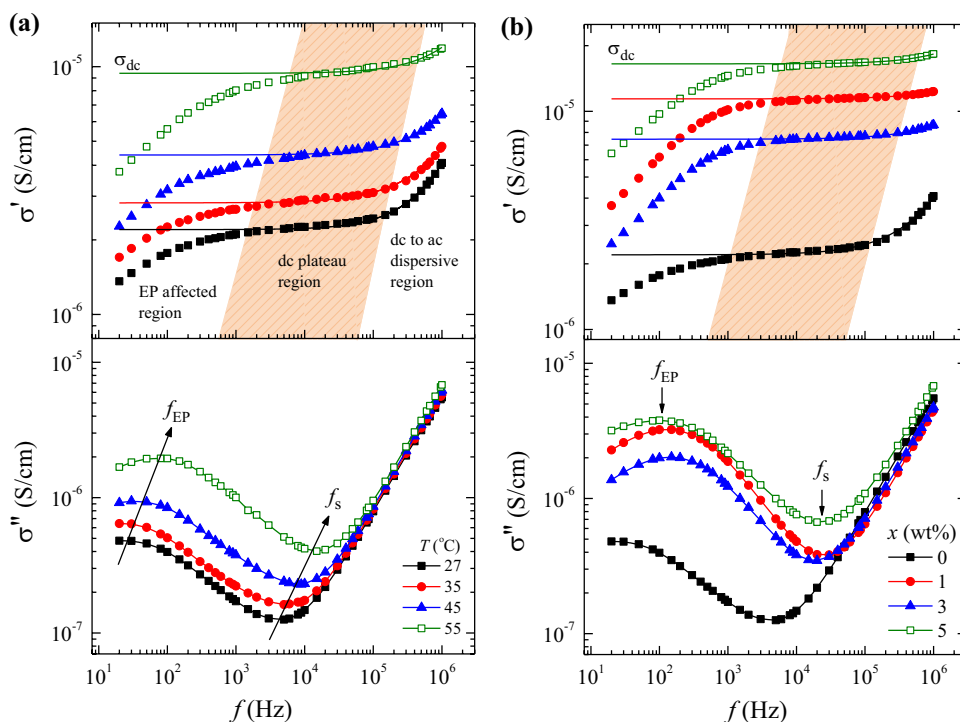
Figure 6a shows the σ' and σ'' spectra of (PEO–PMMA)–13.3 wt% LiBF_4 film at different temperatures, whereas, the MMT concentration dependent these spectra of the NSPE films at 27 °C are shown in Fig. 6b. Over the frequency range from 20 Hz to 1 MHz, the dispersion of σ' spectra of these films exhibit three distinct regions associated with different phenomena which are marked and highlighted in the figure. The low frequency region in which the σ' values increase non-linearly with the increase of frequency is attributed to the EP effect dominated region in which the accumulation of ions at the electrolyte/electrode interface takes place and form the space charge layers known as electric double layers (EDLs). The intermediate frequency range of the spectra where σ' values remain frequency independent represents the dc plateau region in which the long-range charge

carriers diffusion occurs via hopping. The high frequency region of the spectra above the dc plateau range, where the σ' values increase non-linearly, attributes to the dc to ac dispersive region of these electrolyte materials. This type of dispersion behaviour of the σ' spectra is a common characteristic of numerous SPE, NSPE, and PSPE materials reported earlier [17, 19, 29–32, 35–38, 42, 43, 45–50].

The σ' values starting from onset frequency region of dc plateau and ending at 1 MHz for the dc to ac dispersive region of the σ' spectra of SPE and NSPE films were fitted to the Jonscher's power law $\sigma'(\omega) = \sigma_{dc} + A\omega^n$. The σ_{dc} values and the fractional exponent n values obtained from the power law fit of σ' spectra (shown by solid lines in the Fig. 6) for the SPE film at different temperatures and the NSPE films of different concentrations of MMT, at 27 °C, are recorded in Table 2. It can be seen from Table 2 that the σ_{dc} value of SPE film gradually increases with the increase of temperature, whereas for the NSPE films, the σ_{dc} value abruptly increases on the incorporation of 1 wt% MMT and exhibit an anomalous behaviour with the further increase of MMT concentration up to 5 wt%. The n values of these electrolyte films are lower than unity confirming that the ion transportation in these solid ion–dipolar complexes takes place through hopping mechanism as noted in the numerous ion conducting polymeric electrolyte materials [17, 31–35, 49, 51, 52].

The σ'' spectra of the SPE and NSPE films (depicted in the lower layers of Fig. 6) exhibit relaxation peaks in the low frequency region which attribute to the EP relaxation

Fig. 6 The ac electrical conductivity (real part σ' and loss part σ'') spectra of **a** (PEO–PMMA)–13.3 wt% LiBF_4 SPE-film at various temperatures, and **b** (PEO–PMMA)–13.3 wt% LiBF_4 – x wt% MMT NSPE-films at 27 °C



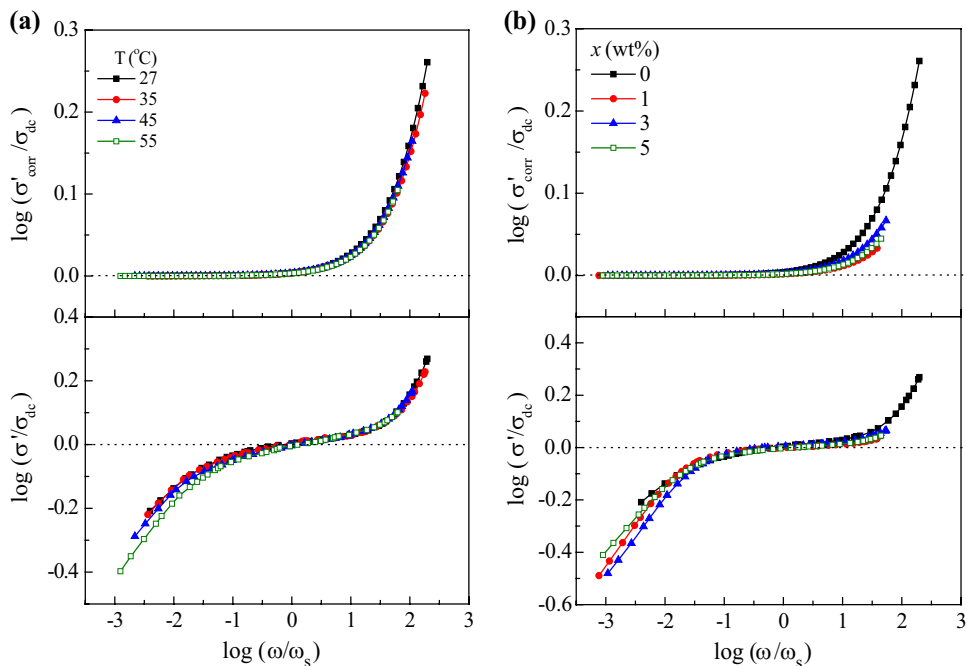
process i.e., corresponding to the dynamics of charging and discharging of EDLs in electrolyte materials [19, 35, 36, 40, 48, 49]. Further, the contribution of EP process starts at onset frequency which is corresponding to dip in the σ'' spectra and the full development of this process occurs at the relaxation peak which is in accordance to the earlier results on the SPE materials [19, 35, 48, 49]. The earlier studies confirmed that the EDL process of the solid electrolytes also has a correlation with the dynamics of polymer chain segmental motion which governs the ions mobility in the complex structures [35, 36, 40]. It is further noted from Fig. 6a that the σ'' values over the EP effect dominated region enhance significantly as the temperature of the film increases. It can be noted from the figure that the peaks of EP process shift towards higher frequencies (as marked by an arrow on the spectra in the figure) with the increase in temperature of the SPE film confirming the temperature activated behaviour of the EDL dynamics of this film. For the NSPE films, the EP relaxation peaks are observed at slightly higher frequency side as compared to that of the SPE film confirming faster relaxation dynamics of the EDLs in the presence of MMT nanofiller. The relaxation times τ_{EDL} for the SPE film with temperature variation and the NSPE films with the increase of MMT concentration were determined from the f_{EP} values using the relation $\tau_{EDL} = 1/2\pi f_{EP}$ and the observed values of τ_{EDL} for these films are recorded in Table 2. In the intermediate frequency range, these σ'' spectra have a minimum (dip) at frequencies marked as f_s and it is revealed that these frequencies are exactly the same as that of the $\tan\delta$ peaks frequencies. These findings confirm that the σ'' spectra can be used to

explore the dynamics of EDL and also of the polymer chain segments in the ion–dipolar complexes of solid electrolytes. Further, the f_s values also denote the onset frequencies of the EP effect from where the contribution of EP process starts and after that, it enhances with a decrease of frequency and its full development takes place at f_{EP} . In addition to these facts, the σ'' values of the SPE and NSPE films initially show a non-linear increase with the increase of frequency from f_s but shortly turn to linear behaviour which is governed by the polymers dipolar relaxation process. This linear behaviour of σ'' values is known as nearly constant loss (NCL) region where the dielectric loss remains nearly frequency independent as demonstrated earlier for the SPE materials [19, 48].

3.2.3 Scaling of ac conductivity spectra

The scaling of σ' spectra at different temperatures for the (PEO–PMMA)–13.3 wt% LiBF₄ film and also of different MMT concentration for the (PEO–PMMA)–13.3 wt% LiBF₄–*x* wt% MMT films at 27 °C are depicted in Fig. 7 in the scaling formalism (the σ' axis is scaled by σ_{dc} and the ω axis is scaled by ω_s , where $\omega = 2\pi f$ and $\omega_s = 2\pi f_s$). The upper layers of Fig. 7a, b represent the EP effect corrected values of scaled conductivity of the electrolyte films. The upper layer of Fig. 7a confirms the superposition of different temperature conductivity spectra on a common master curve which reveals that the dynamical processes involved in the SPE film obey the time–temperature superposition principle. The actual values of conductivity scaled spectra of the SPE film (lower layer of Fig. 7a) reveal that they do

Fig. 7 The log–log σ' spectra scaling of **a** (PEO–PMMA)–13.3 wt% LiBF₄ SPE-film at various temperatures, and **b** (PEO–PMMA)–13.3 wt% LiBF₄–*x* wt% MMT NSPE-films at 27 °C



not fall on a single master curve in the EP effect dominated low frequency region. Similar nature of conductivity scaled spectra has also been obtained for several electrolyte materials [40, 43, 47, 51]. This time–temperature scaling behaviour of conductivity indicates that the mechanism of ions successful hopping with reduced mismatching is true for the SPE film throughout the temperature range of 27–55 °C. Figure 7b shows that the superposition of ac conductivity spectra for different composition NSPE films falls on a common master curve up to the dc plateau region for the corrected conductivity scale spectra (upper layer of Fig. 7b) and only over the limited dc plateau region for the actual conductivity scaled spectra (lower layer of Fig. 7b). This scaling behaviour of NSPE films of different MMT concentration infers that the relaxation mechanism in these films is compositional dependent.

3.2.4 Relaxation time dependence of ionic conductivity

The σ_{dc} of an ionic conductor is related to the charge of moving ions q_i , ions mobility μ_i , and the ions concentration n_i by the relation $\sigma_{dc} = \sum q_i \mu_i n_i$. The XRD study of these electrolyte films confirmed that the added LiBF_4 amount has completely dissociated in its monovalent cations Li^+ and anions BF_4^- because there is absence of diffraction peaks of the crystalline salt in the XRD patterns of the films. Therefore, for these NSPE materials, the q_i and n_i values are fixed and the variation in σ_{dc} values is mainly due to the changes in μ_i values. Figure 8 shows the MMT concentration dependent τ_{EDL} , τ_s and σ_{dc} plots of NSPE films at 27 °C. Both the τ_s and τ_{EDL} values of NSPE films are found significantly low as compared to that of the SPE film without MMT, and there is little variation in these relaxation times with the change of MMT concentration in the range from 1 to 5 wt% in the films. Further, there is about two orders of magnitude difference in the observed τ_s and τ_{EDL} values of these electrolyte films. From Fig. 8, it can be clearly noted that the σ_{dc} of NSPE films are about one order of magnitude high as compared to that of the SPE film at the same temperature. The σ_{dc} values for these NSPE films also increase as a result of the decrease in τ_s values. From this correlation of the σ_{dc} and τ_s values, it can be concluded that the ions transport occurs coupled with the dynamics of polymer chain segments. The increase of chain segmental dynamics (i.e., the decrease of τ_s) accelerates the ions mobility and hence there is an increase of ionic conductivity of the NSPE films. This fact is true at all the MMT concentrations of the NSPE films as revealed from the inverse relation found between the respective σ_{dc} and τ_s values at the room temperature. The MMT has been used by several investigators as an inorganic nanofiller for the preparation of various kinds of NSPE materials [27, 32, 34, 36, 53–55] in view of the fact that MMT enhances the thermal and

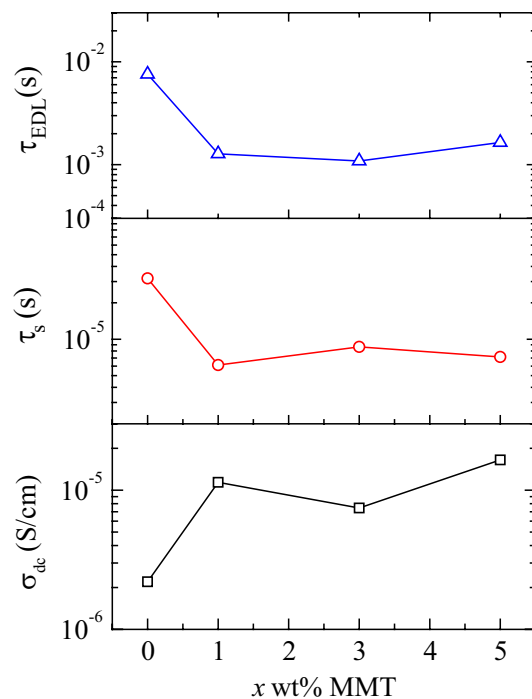


Fig. 8 MMT concentration dependent dc ionic conductivity σ_{dc} , polymer chain segmental dynamics relaxation time τ_s , and EDL relaxation time τ_{EDL} of the (PEO–PMMA)–13.3 wt% LiBF_4 –x wt% MMT films at 27 °C

mechanical stability of such material. But the intercalated MMT structures accelerate the ions transport mechanism through the formation of favourable ion conducting paths, and the exfoliated MMT prevents the ion-pairing effect due to their high aspect ratio, which all are important properties for performance enhancement of the MMT dispersed electrolyte materials [30–34, 36]. The XRD study of these NSPE films revealed that there is relatively more amount of intercalated phases in 3 wt% MMT containing NSPE film but its conductivity value is slightly low as compared to the 1 and 5 wt% MMT containing NSPE films with a higher amount of MMT exfoliated phases. This finding reveals that the dynamics of polymer chain segments in the ion–dipolar complexes has a dominant effect on the conductivity enhancement in these NSPE materials. In regards to the confirmation of structural dynamics in the solid polymer electrolytes, DRS is a powerful technique and it is frequently employed by several investigators [17–20, 29–36, 47, 48]. But recently time-resolved Fourier transform infrared (TR-FTIR) combined with two-dimensional correlation FTIR (2D-COR-FTIR) spectroscopy has been used for real-time tracking of the Li^+ -ion transition behaviour and dynamics in SPE materials under an external electric field [28]. Results reported on the SPEs using this characterization technique are very interesting in regards to the detailed demonstration of the ion transport mechanism in

the SPE materials. It was reported that the Li^+ migration in the SPEs under an external electric field is a highly complicated process which includes quasi-periodic dissociation and coordination effects between Li^+ -ion carriers and the dynamical polymeric chains. These quasi-periodic dissociation times for the SPEs are found of the order of few μs duration [28], and these times durations are in agreement with the relaxation time of ions coupled polymer chain segmental dynamics of numerous SPE materials which were determined from the DRS technique [29–36, 47, 48]. Therefore, in general, the DRS measurements give the correct idea regarding the ions transportation mechanism in the SPE materials.

Further, From Table 2, it can be noted that the σ_{dc} values of the SPE film increase and the τ_s values decrease with the increase of film temperature which also confirms that the mobility of ions enhances due to the increase of polymer segmental dynamics in the thermally activated solid ion–dipolar matrix. A similar correlation between the σ_{dc} and τ_s values has also been reported for various SPE, NSPE and PSPE materials investigated by employing the DRS technique [17–20, 27, 29–38, 43, 47, 48, 50, 56]. Furthermore, the correlation between σ_{dc} and τ_{EDL} has also been found for these NSPE materials, which reveals that there is contribution of the EDL dynamics in the σ_{dc} values which is in addition to the dynamics of polymer chain segments.

3.2.5 Arrhenius behaviour

The plots of logarithmic σ_{dc} , τ_s , and τ_{EDL} values versus $1000/T$ are shown in Fig. 9 which exhibit linear behaviour for the (PEO–PMMA)–13.3 wt% LiBF_4 film. For the comparison, the plots of the same parameters of the (PEO–PMMA)–9.7 wt% LiBF_4 film are also added in the figure. The temperature dependent values of these parameters obey the Arrhenius relations $\sigma_{\text{dc}} = \sigma_0 \exp(-E_\sigma/k_B T)$ for the conductivity activation energy E_σ , and $\tau = \tau_0 \exp(E_\tau/k_B T)$ for the relaxation time activation energy E_τ . The temperature dependent σ_{dc} , τ_s , and τ_{EDL} values for the (PEO–PMMA)–9.7 wt% LiBF_4 film were taken from our earlier study [40]. The E_σ and E_τ values were determined from the slopes of these parameters linear plots, and the obtained activation energy values are marked in the figure. For both the salt concentrations (i.e., 9.7 and 13.3 wt%) SPE films, their E_σ values are found slightly higher than that of the E_τ values and these values are relatively high for the SPE film containing the higher concentration (13.3 wt%) of salt (i.e., $\text{E}\dd{\text{O}} + \text{C}=\dd{\text{O}}$): $\text{Li}^+ = 12:1$). In case of SPE materials, the E_σ is attributed as the sum of energies required for breaking the Li^+ ion–polymer interaction and then for Li^+ hopping [57]. Lower E_σ value confirms the transient-type Li^+ ion–polymer interaction which has ease of breaking and faster hopping of ions in the solid ion–dipolar complexes [37], and this type of ion

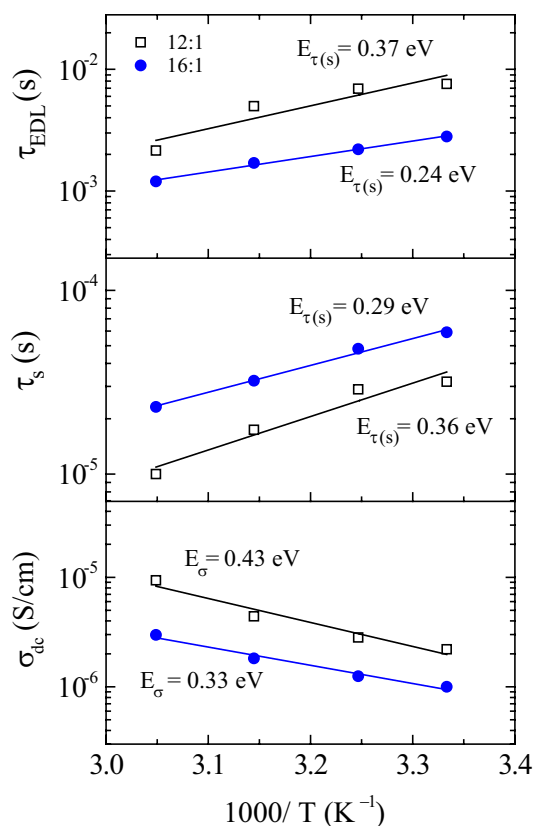


Fig. 9 Temperature dependent Arrhenius plots of dc ionic conductivity σ_{dc} , polymer chain segmental dynamics relaxation time τ_s , and EP relaxation time τ_{EDL} for the (PEO–PMMA)–13.3 wt% LiBF_4 film of stoichiometric molar ratio 12:1 and the (PEO–PMMA)–9.7 wt% LiBF_4 film of stoichiometric molar ratio 16:1

transportation mechanism also occurs in the studied SPE film as revealed from its low E_σ value. The slightly higher E_σ value as compared to E_τ value reveals that more energy is needed for the ions to crossover the potential barrier during the conduction as compared to that of the relaxation in these SPE materials. Further, the observed E_σ and E_τ values of these SPE films are also found in good agreement with earlier reported values for different SPE, NSPE and PSPE materials [19, 21, 31, 37, 44, 45, 48, 50, 52, 56].

3.3 Electrochemical performance

3.3.1 Linear sweep voltammetry (LSV)

The electrochemical stability window (ESW) i.e., the working voltage limit is one of the important parameters of an electrolyte material for confirmation of its energy storing device applications. The ESW values of the (PEO–PMMA)–13.3 wt% LiBF_4 – x wt% MMT films were estimated from their LSV plots given in Fig. 10. For the LSV characterization, the S-cell assembly of the SS

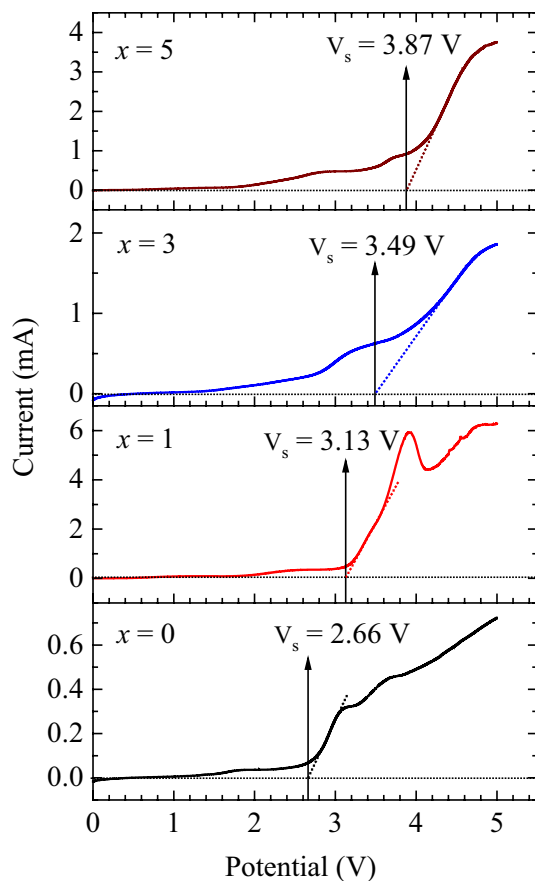


Fig. 10 Linear sweep voltammograms (LSV) of (PEO-PMMA)-13.3 wt% LiBF_4 - x wt% MMT films for $x=0, 1, 3,$ and 5 recorded using SS||NSPE||SS symmetric blocking cell (S-cell) at room temperature. The values of V_s for these NSPEs are marked in the respective plots

electrodes and electrolyte was used which is an alternative appropriate arrangement for the electrochemical testing of a solid electrolyte material [18, 39, 40, 58, 59], without fabricating a lithium-cell [60]. From Fig. 10, it can be noted that the residual electronic current is almost zero initially, but it slowly increases with increasing the applied voltage across the S-cell up to a certain voltage V_s and beyond that current increase sharply. The V_s values for these NSPE films are marked in the figure from the tangent drawn on abrupt rise part of the LSV plot and its intersection at the zero current. The ESW values of these NSPE can be taken equal to twice of V_s . It is found that V_s values gradually enhance with the increase of MMT concentration in the NSPE films and it is about 3.9 V for the 5 wt% MMT containing NSPE film. The V_s values are significantly high confirming the suitability of these NSPE films to use as solid state separator/electrolytes in the fabrication of solid-state Li-ion batteries [18].

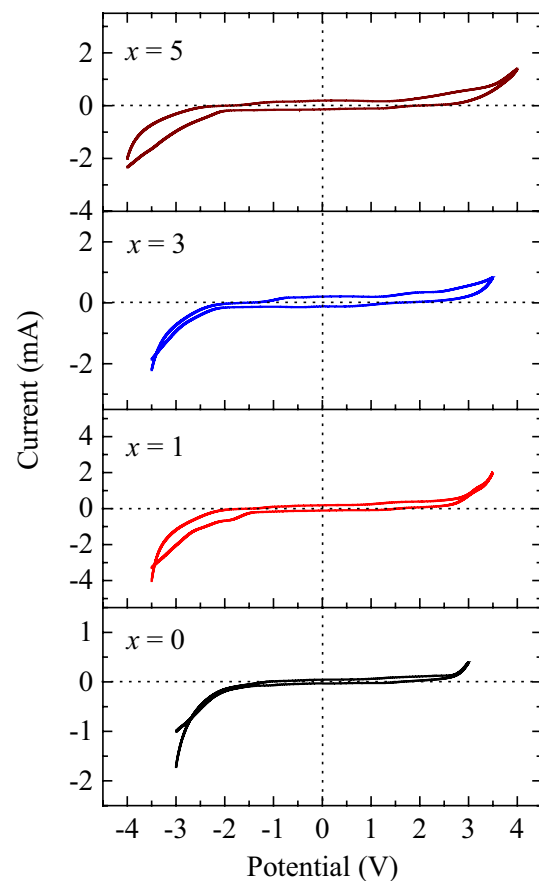


Fig. 11 Cyclic voltammograms (CV) of (PEO-PMMA)-13.3 wt% LiBF_4 - x wt% MMT films for $x=0, 1, 3,$ and 5 , at room temperature

3.3.2 Cyclic voltammetry

The cyclic voltammetry (CV) traces of the NSPE films performed with S-cell assembly over the ESW range, at room temperature, are depicted in Fig. 11. The symmetry of the CV traces confirms that these NSPE films bear excellent reversibility and cyclability over the ESW range. There are no anodic and cathodic peaks in these CV traces of the NSPE films which is an evidence of non-interactive behaviour of cations (Li^+) with the SS-blocking electrodes. The shapes of CV traces of these NSPE electrolyte films were also found in good agreement with the earlier reported results on various SPE materials [18, 39, 40, 58, 59].

3.3.3 Chronoamperometry

The chronoamperograms (CA) of the NSPE films are depicted in Fig. 12, which shows that the initial current I_0 decreases non-linearly with the increase of time and finally approaches steady state I_{ss} . The total ion transfer number t_{ion} of the NSPE films were determined using the relation $t_{ion} = 1 - (I_{ss}/I_0)$ [11, 39, 40, 59]. For these ion

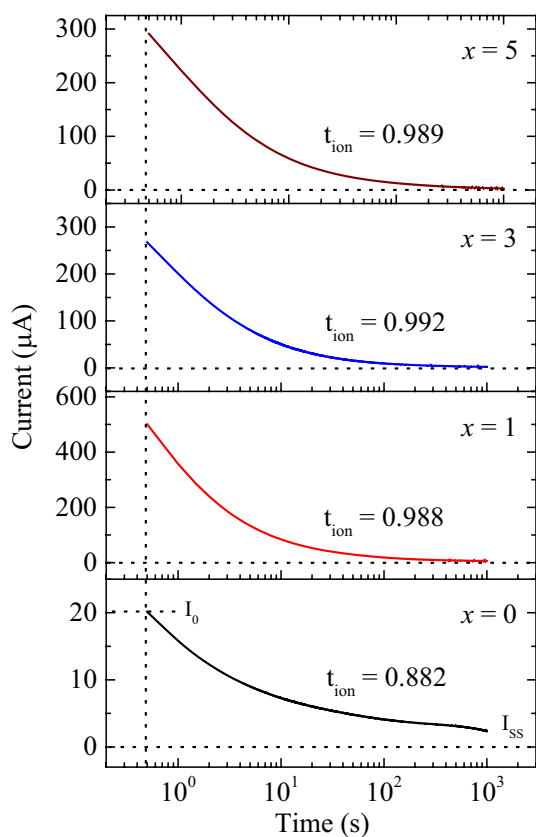


Fig. 12 Chronoamperograms (CA) of (PEO-PMMA)-13.3 wt% LiBF_4 - x wt% MMT films for $x=0, 1, 3,$ and 5 , at room temperature. The t_{ion} values for these NSPEs are given in the respective plots

conducting materials, the electronic transference number t_e is considered equal to $1 - t_{\text{ion}}$. The t_{ion} values for the NSPE films were marked in the figure. The t_{ion} values for the NSPEs films were found close to unity confirming that the total electrical conductivity is predominantly ionic.

4 Conclusions

The effects of LiBF_4 salt concentration and MMT nanofiller concentration on the structural, dielectric and electrical properties of the (PEO-PMMA)-9.7 wt% LiBF_4 and (PEO-PMMA)-13.3 wt% LiBF_4 - x wt% MMT films have been reported. These SPE and NSPE films are predominantly amorphous and the NSPE films have both the intercalated and exfoliated MMT phases. The formation of ion-dipolar-nanofiller coordination mainly suppresses the crystalline phase of PEO in these NSPE films. The ionic conductivity of the SPE films increases 2.2 times when the salt concentration increases from 9.7 to 13.3 wt%, and it further increases by about one order of magnitude for the 5 wt% MMT incorporated NSPE film at room temperature. The dominant phase of exfoliated MMT structures and

relatively faster dynamics of the polymer chain segments accelerates the ions mobility through hopping mechanism which results in an increase of the ionic conductivity of the NSPE films. A close coupling between the conduction of ions and relaxation time for polymer chain segmental dynamics is observed for all these electrolytes materials. The low activation energies are observed for the conductivity and relaxation time of the SPE films. These NSPE films have high ESW, good reversibility, and cyclability, and the total ion transference number is close to unity. The ambient temperature ionic conductivity values of the NSPE films are of the order of 10^{-5} S/cm and they exhibit reasonably appropriate values of electrochemical performance parameters, confirming them as a potential candidate for the ion conductor/separator in the fabrication of rechargeable solid-state lithium-ion batteries, and also for the numerous ion conducting electrochemical devices.

Acknowledgements One of the authors (PD) thanks to the CSIR, New Delhi for the award of a postdoctoral research associate fellowship. The authors are thankful to Dr. J. S. Rathore, Department of Chemistry, Jai Narain Vyas University Jodhpur, for extending FTIR facility.

Funding The authors gratefully acknowledge financial support from the Government of Rajasthan, Jaipur, through RUSA Grant No. F30(16)SPD/RUSA/2016/218 for setting the facility of the electrochemical analyzer.

Compliance with ethical standards

Conflict of interest The authors declare that they have no conflict of interest.

References

- Scrosati B, Hassoun J, Sun Y-K (2011) Lithium-ion batteries. A look into the future. *Energy Environ Sci* 4:3287–3295
- Korthauer R (2018) Lithium-ion batteries: basics and applications. Springer, Berlin
- Liu B, Zhang J-G, Xu W (2018) Advancing lithium metal batteries. *Joule* 2:833–845
- Yan L, Wang H, Huang D, Luo H (2018) Electrodes with high conductivities for high performance lithium/sodium ion batteries. *Eng Sci* 1:4–20
- Zhao B, Ran R, Liu M, Shao Z (2015) A comprehensive review of $\text{Li}_4\text{Ti}_5\text{O}_{12}$ -based electrodes for lithium-ion batteries: the latest advancements and future perspectives. *Mater Sci Eng R Rep* 98:1–71
- Xue Z, He D, Xie X (2015) Poly(ethylene oxide)-based electrolytes for lithium-ion batteries. *J Mater Chem A* 3:19218–19253
- Long L, Wang S, Xiao M, Meng Y (2016) Polymer electrolytes for lithium polymer batteries. *J Mater Chem A* 4:10038–10069
- Yue L, Ma J, Zhang J, Zhao J, Dong S, Liu Z, Cui G, Che L (2016) All solid-state polymer electrolytes for high-performance lithium ion batteries. *Energy Storage Mater* 5:139–164
- Ngai KS, Ramesh S, Ramesh K, Juan JC (2016) A review of polymer electrolytes: fundamental, approaches and applications. *Ionics* 22:1259–1279

10. Mindemark J, Lacey MJ, Bowden T, Brandell D (2018) Beyond PEO—alternative host materials for Li^+ -conducting solid polymer electrolytes. *Prog Polym Sci* 81:114–143
11. Arya A, Sharma AL (2017) Insights into the use of polyethylene oxide in energy storage/conversion devices: a critical review. *J Phys D Appl Phys* 50:443002
12. Glynos E, Petropoulou P, Mygiakis E, Nega AD, Pan W, Papoutsakis L, Giannelis EP, Sakellariou G, Anastasiadis SH (2018) Leveraging molecular architecture to design new, all-polymer solid electrolytes with simultaneous enhancement in modulus and ionic conductivity. *Macromolecules* 51:2542–2550
13. Zhang B, Tan R, Yang L, Zheng J, Zhang K, Mo S, Lin Z, Pan F (2018) Mechanisms and properties of ion-transport in inorganic solid electrolytes. *Energy Storage Mater* 10:139–159
14. Karim SRA, Sim LH, Chan CH, Ramli H (2015) On thermal and spectroscopic studies of poly(ethylene oxide)/poly(methyl methacrylate) blends with lithium perchlorate. *Macromol Symp* 354:374–383
15. Keller M, Varzi A, Passerini S (2018) Hybrid electrolytes for lithium metal batteries. *J Power Sources* 392:206–225
16. Amiri H, Mohsennia M (2017) Impedance study of PVA/PEG/ $\text{LiClO}_4/\text{TiO}_2$ nanocomposite solid polymer electrolyte. *J Mater Sci Mater Electron* 28:4586–4592
17. Dam T, Tripathy SN, Paluch M, Jena SS, Pradhan DK (2016) Investigations of relaxation dynamics and observation of nearly constant loss phenomena in $\text{PEO}_{20}\text{-LiCF}_3\text{SO}_3\text{-ZrO}_2$ based polymer nano-composite electrolyte. *Electrochim Acta* 202:147–156
18. Sengwa RJ, Dhatarwal P, Choudhary S (2018) Study of time-ageing effect on the ionic conduction and structural dynamics in solid polymer electrolytes by dielectric relaxation spectroscopy. *Solid State Ion* 324:247–259
19. Pal P, Ghosh A (2018) Influence of TiO_2 nano-particles on charge carrier transport and cell performance of PMMA– LiClO_4 based nano-composite electrolytes. *Electrochim Acta* 260:157–167
20. Das S, Ghosh A (2015) Effect of plasticizers on ionic conductivity and dielectric relaxation of PEO– LiClO_4 polymer electrolyte. *Electrochim Acta* 171:59–65
21. Polu AR, Rhee HW, Kim DK (2015) New solid polymer electrolytes ($\text{PEO}_{20}\text{-LiTfDI-SN}$) for lithium batteries: structural, thermal and ionic conductivity studies. *J Mater Sci Mater Electron* 26:8548–8554
22. Duan H, Yin Y-X, Zeng X-X, Li J-Y, Shi J-L, Shi Y, Wen R, Guo Y-G, Wan L-J (2018) In-situ plasticized polymer electrolyte with double-network for flexible solid-state lithium-metal batteries. *Energy Storage Mater* 10:85–91
23. Genovese M, Wu H, Virya A, Li J, Shen P, Lian K (2018) Ultrathin all-solid-state supercapacitor devices based on chitosan activated carbon electrodes and polymer electrolytes. *Electrochim Acta* 273:392–401
24. Venkatesan S, Liu I-P, Lin J-C, Tsai M-H, Teng H, Lee Y-L (2018) Highly efficient quasi-solid-state dye-sensitized solar cell using polyethylene oxide (PEO) and poly(methyl methacrylate) (PMMA)-based printable electrolytes. *J Mater Chem A* 6:10085–10094
25. Zhang HW, Shen PK (2012) Recent development of polymer electrolyte membranes for fuel cells. *Chem Rev* 112:2780–2832
26. Thakur VK, Ding G, Ma J, Lee PS, Lu X (2012) Hybrid materials and polymer electrolytes for electrochromic device applications. *Adv Mater* 24:4071–4096
27. Dam T, Karan NK, Thomas R, Pradhan DK, Katiyar RS (2015) Observation of ionic transport and ion-coordinated segmental motions in composite (polymer-salt-clay) solid polymer electrolyte. *Ionics* 21:401–410
28. Bao L, Zou X, Luo X, Pu Y, Wang J, Lei J (2017) Real-time tracking the Li^+ -ion transition behaviour and dynamics in solid poly(vinyl alcohol)/ LiClO_4 electrolytes. *Sci Rep* 7:45921
29. Choudhary S, Sengwa RJ (2013) Effects of preparation methods on structure, ionic conductivity and dielectric relaxation of solid polymeric electrolytes. *Mater Chem Phys* 142:172–181
30. Sengwa RJ, Choudhary S (2014) Dielectric properties and fluctuating relaxation processes of poly(methyl methacrylate) based polymeric nanocomposite electrolytes. *J Phys Chem Solids* 75:765–774
31. Sengwa RJ, Dhatarwal P, Choudhary S (2014) Role of preparation methods on the structural and dielectric properties of plasticized polymer blend electrolytes: correlation between ionic conductivity and dielectric parameters. *Electrochim Acta* 142:359–370
32. Sengwa RJ, Dhatarwal P, Choudhary S (2015) Effects of plasticizer and nanofiller on the dielectric dispersion and relaxation behaviour of polymer blend based solid polymer electrolytes. *Curr Appl Phys* 15:135–143
33. Choudhary S, Sengwa RJ (2015) Structural and dielectric studies of amorphous and semicrystalline polymers blend-based nanocomposite electrolytes. *J Appl Polym Sci* 132:41311
34. Sengwa RJ, Choudhary S, Dhatarwal P (2015) Influences of ultrasonic- and microwave-irradiated preparation methods on the structural and dielectric properties of (PEO–PMMA)– $\text{LiCF}_3\text{SO}_3\text{-x wt\% MMT}$ nanocomposite electrolytes. *Ionics* 21:95–109
35. Dhatarwal P, Sengwa RJ (2017) Dielectric and electrical characterization of (PEO–PMMA)– $\text{LiBF}_4\text{-EC}$ plasticized solid polymer electrolyte films. *J Polym Res* 24:135
36. Dhatarwal P, Sengwa RJ, Choudhary S (2017) Effect of intercalated and exfoliated montmorillonite clay on the structural, dielectric and electrical properties of plasticized nanocomposite solid polymer electrolytes. *Compos Commun* 5:1–7
37. Choudhary S, Sengwa RJ (2017) Effects of different inorganic nanoparticles on the structural, dielectric and ion transportation properties of polymers blend based nanocomposite solid polymer electrolytes. *Electrochim Acta* 247:924–941
38. Dhatarwal P, Sengwa RJ (2017) Effects of PEG plasticizer concentrations and film preparation methods on the structural, dielectric and electrical properties of PEO–PMMA blend based plasticized solid polymer electrolyte films. *Indian J Pure Appl Phys* 55:7–18
39. Dhatarwal P, Choudhary S, Sengwa RJ (2018) Electrochemical performance of Li^+ -ion conducting solid polymer electrolytes based on PEO–PMMA blend matrix incorporated with various inorganic nanoparticles for the lithium ion batteries. *Compos Commun* 10:11–17
40. Dhatarwal P, Sengwa RJ (2018) Influence of solid polymer electrolyte preparation methods on the performance of (PEO–PMMA)– LiBF_4 films for lithium-ion battery applications. *Polym Bull* 75:5645–5666
41. Choudhary S, Sengwa RJ (2014) Intercalated clay structures and amorphous behavior of solution cast and melt pressed poly(ethylene oxide)–clay nanocomposites. *J Appl Polym Sci* 131:39898
42. Shukla N, Thakur AK, Shukla A, Chatterjee R (2014) Dielectric relaxation and thermal studies on dispersed phase polymer nanocomposite films. *J Mater Sci Mater Electron* 25:2759–2770
43. Morsi MA, El-Khodary SA, Rajeh A (2018) Enhancement of the optical, thermal and electrical properties of PEO/PAM: Li polymer electrolyte films doped with Ag nanoparticles. *Phys B Condens Matter* 539:88–96
44. Hebbar V, Bhajantri RF, Naik J (2017) Physico-chemical properties of Bismuth nitrate filled PVA– LiClO_4 polymer composites for energy storage applications. *J Mater Sci Mater Electron* 28:5827–5839
45. Duraikkan V, Sultan AB, Nallaperumal N, Shunmuganarayanan A (2018) Structural, thermal and electrical properties of polyvinyl

- alcohol/poly(vinyl pyrrolidone)–sodium nitrate solid polymer blend electrolyte. *Ionics* 24:139–151
46. Aziz SB, Abdullah OGh, Rasheed MA (2017) Structural and electrical characteristics of PVA:NaTf based solid polymer electrolytes: role of lattice energy of salts on electrical conductivity. *J Mater Sci Mater Electron* 28:12873–12884
 47. Dam T, Jena SS, Pradhan DK (2018) Coupled ion conduction mechanism and dielectric relaxation phenomenon in PEO₂₀–LiCF₃SO₃-based ion conducting polymer nanocomposite electrolytes. *J Phys Chem C* 122:4133–4143
 48. Pal P, Ghosh A (2018) Investigation of ionic conductivity and relaxation in plasticized PMMA–LiClO₄ solid polymer electrolytes. *Solid State Ionics* 319:117–124
 49. Ravi M, Song S, Wang J, Wang T, Nadimicherla R (2016) Ionic liquid incorporated biodegradable gel polymer electrolyte for lithium ion battery applications. *J Mater Sci Mater Electron* 27:1370–1377
 50. Manjunatha H, Damle R, Pravin K, Kumaraswamy GN (2018) Modification in the transport and morphological properties of solid polymer electrolyte system by low-energy ion irradiation. *Ionics* 24:3027–3037
 51. Nath AK, Kumar A (2014) Scaling of AC conductivity, electrochemical and thermal properties of ionic liquid based polymer nanocomposite electrolytes. *Electrochim Acta* 129:177–186
 52. Pavani Y, Ravi M, Bhavani S, Karthikeya RS, Narasimha Rao VVR (2018) Physical investigations on pure and KBr doped poly(vinyl alcohol) (PVA) polymer electrolyte films for solid state battery applications. *J Mater Sci Mater Electron* 29:5518–5524
 53. Shukla N, Thakur AK (2010) Ion transport model in exfoliated and intercalated polymer–clay nanocomposites. *Solid State Ionics* 181:921–932
 54. Deka M, Kumar A (2010) Enhanced electrical and electrochemical properties of PMMA–clay nanocomposite gel polymer electrolytes. *Electrochim Acta* 55:1836–1842
 55. Deka M, Kumar A (2013) Dielectric and conductivity studies of 90 MeV O⁷⁺ ion irradiated poly(ethylene oxide)/montmorillonite based ion conductor. *J Solid State Electrochem* 17:977–986
 56. Ganesan SV, Mothilal KK, Selvasekarapandian S, Ganesan TK (2018) The effect of titanium dioxide nano-filler on the conductivity, morphology and thermal stability of poly(methyl methacrylate)—poly(styrene-co-acrylonitrile) based composite solid polymer electrolytes. *J Mater Sci Mater Electron* 29:8089–8099
 57. Mohapatra SR, Nair MG, Thakur AK (2018) Synergistic effect of nano-ceria dispersion on improvement of Li⁺ ion conductivity in polymer nanocomposite electrolytes. *Mater Lett* 221:232–235
 58. Rocco AM, Pereira RP (2015) Solid electrolytes based on poly(ethylene oxide)/poly(4-vinyl phenol-co-2-hydroxyethyl methacrylate) blends and LiClO₄. *Solid State Ionics* 279:78–89
 59. Arya A, Sharma AL (2018) Structural, microstructural and electrochemical properties of dispersed type polymer nanocomposite films. *J Phys D Appl Phys* 51:045504
 60. Nair JR, Colò F, Kazzazi A, Moreno M, Bresser D, Lin R, Bella F, Meligrana G, Fantini S, Simonetti E, Appetecchi GB, Passerini S, Gerbaldi C (2019) Room temperature ionic liquid (RTIL)-based electrolyte cocktails for safe, high working potential Li-based polymer batteries. *J Power Sources* 412:398–407